International Journal of Fatigue 176 (2023) 107887

Contents lists available at ScienceDirect

International Journal of Fatigue

journal homepage: www.elsevier.com/locate/ijfatigue

A new method for ultrasonic fatigue component frequency modulation: From ultrasonic horn to uniaxial and multiaxial specimens

Pedro R. da Costa [a,b], Masoud Rahaeifard [c], Diogo Montalvão [d,*], Luís Reis [b], Manuel Freitas [a,b]

[a] Atlântica, Instituto Universitário, Fábrica de Pólvora de Barcarena, 2730-036 Barcarena, Portugal
[b] IDMEC, Instituto Superior Técnico, Universidade de Lisboa, Av. Rovisco Pais, 1, 1050-099 Lisboa, Portugal
[c] Department of Mechanical Engineering, Faculty of Engineering, Ardakan University, P.O. Box 184, Ardakan, Iran
[d] Department of Design and Engineering, Faculty of Science and Technology, Bournemouth University, Poole House, Talbot Campus, Fern Barrow, Poole BH12 5BB, United Kingdom

ARTICLE INFO

Keywords:
Ultrasonic Fatigue Testing (UFT)
Specimen design
Uniaxial fatigue
Multiaxial fatigue
Very High Cycle Fatigue (VHCF)

ABSTRACT

Ultrasonic fatigue specimens require rigorous design. The entire machine and specimen setup must vibrate in resonance at high frequencies, with the desired mode shapes that produce the intended stresses. The connection between parts must be considered too as they should allow for the desired mode shape to vibrate in free-free conditions. Most published research uses an analytical method that works only for uniaxial tension–compression or pure torsion specimens. This limits the range of experiments. In this paper, a semi-analytical formulation that can model more complex ultrasonic specimen geometries for a variety of stress states is proposed, namely multiaxial tension–torsion. Comparing numerical simulations with the analytical method show a good correlation between results. This work can help other researchers to design and conduct more varied and efficient ultrasonic fatigue experiments.

1. Introduction

Fatigue characterisation has become more complex and nuanced over the years. From uniaxial sinusoidal cyclic loading to complex cyclic loading, to multiaxial fatigue, to corrosion, to fretting, and to many other important variables, fatigue testing has reached a level of complexity that the 19th century pioneering work from Wohler could never anticipate. The goal of much of the fatigue research today is to describe and measure the fatigue behaviour of materials in a way that is repeatable and scalable. The results can then be used to validate models or to create and improve working engineering standards.

Engineering standards for fatigue testing and characterisation, for example ISO12108:2018 and ASTM E647-23 for fatigue crack growth testing or ISO 12106:2017 and ASTM E606/E606M-21 for strain-controlled methods (among many other standards), define rigorous experimental practices. These standards specify the specimen's geometry, the analytical calculations, and the experimental methodology that must be followed. One novel method under research, which only existing standard, WES 1112:2017, is from the Japan Welding Engineering Society [1,2], is the ultrasonic fatigue testing method. The first Ultrasonic Fatigue Testing (UFT) machine was designed by Mason in 1951 [3]. This machine induced cyclic tension–compression at the groundbreaking 20 kHz frequency. Such high testing frequency allowed to speed up tests to the point that it became possible to study the Very High Cycle Fatigue (VHCF) regime, between 10^6 to 10^{10} cycles.

The UFT method did not attract much attention from the scientific community at first. This was primarily related to the technological challenges of reliably controlling, measuring, and collecting all the necessary experimental data at such high frequencies. Today's advances in computing power, measurement equipment and data acquisition capabilities, have enabled researchers to overcome many of the previous barriers in UFT. This resulted in a vast number of publications being presented in the last 10 to 20 years, new UFT machines being built, novel experimental methodologies being presented, and expanding the capability into a large variety of materials and stress profiles [4]. To the present-day, researchers have achieved tension–compression with and without mean stress [5–7], pure torsion with and without mean stress [8,9], bending with and without mean

Abbreviations: ASTM, American Society for Testing and Materials; FEA, Finite Element Analysis; ISO, International Standards Organisation; ODEs, Ordinary Differential Equations; VHCF, Very High Cycle Fatigue; UTF, Ultrasonic Fatigue Testing; WES, Welding Engineering Society.

* Corresponding author.
E-mail address: dmontalvao@bournemouth.ac.uk (D. Montalvão).

https://doi.org/10.1016/j.ijfatigue.2023.107887
Received 13 June 2023; Received in revised form 22 July 2023; Accepted 12 August 2023
Available online 17 August 2023

stress [10,11], biaxial in-plane tension–compression (from equibiaxial to pure shear) [12,13], biaxial bending [14], and biaxial tension–torsion. Furthermore, such studies were demonstrated using conventional metals [15], additive manufactured metals [16], and/or composite materials [17,18]. There are many more published examples of the variety in UFT machine capabilities.

Regarding uniaxial tension–compression and pure torsion ultrasonic specimens, a well-established analytical method has been vastly used [16]. For bending there are analytical models for ultrasonic 3-point bending fatigue as well. For any other loads or any considerable changes in the specimen's geometry the analytical solution becomes impractical or even unfeasible. The Japanese standard WES 1112:2017 [2] and the book from Bathias and Paul [19] describe the analytical method to design a specimen with resonance at the working frequency of the machine. The equation that relates the point of displacement measurement with the maximum induced stress is also derived.

ptBased on the work from Arani and Rahaeifard [20], the present research proposes a fast semi-analytical approach for frequency, mode shape determination and stress calculations towards ultrasonic fatigue specimen modulation. In this approach, the displacement field is expanded using base functions which satisfy the essential boundary conditions. Utilising this method, the governing equation can be reduced to an eigenvalue algebraic problem which gives natural frequencies, mode shapes and stress distribution throughout the specimen axis. It gives good accuracy and fast responses for specimens with variable cross sections.

This work aims to develop a method that can model complex axisymmetric or plane shapes uniaxial and multiaxial ultrasonic specimen geometries, more reliably and faster than numerical methods. The proposed semi-analytical solution, like the numerical and analytical counterparts, determines a geometry that matches the working frequency of the ultrasonic machine and provides the displacement to stress relation for calibration and control of the fatigue experiment. The method was then transcribed in a MATLAB script that can determine any given specimen geometry's longitudinal and torsional resonant frequencies and their associated mode shapes for demonstration of outcomes.

2. Semi-analytical solution

2.1. Modal analysis

The free vibration governing equation of motion of a bar with variable cross section can be written as:

$$-\frac{\partial}{\partial x}\left(\alpha\frac{\partial u}{\partial x}\right)+\beta\frac{\partial^2 u}{\partial t^2}=0 \tag{1}$$

in which u denotes the longitudinal displacement or the torsion angle along the bar axial direction. Due to the variations in the cross section of the bar, quantities α and β are a function of the longitudinal (i.e. x) direction. These parameters can be expressed as per equations (2) and (3) for longitudinal and torsional vibrations, respectively:

$$\alpha(x)=EA(x);\beta(x)=\rho A(x) \tag{2}$$

$$\alpha(x)=GJ(x);\beta(x)=\rho J(x) \tag{3}$$

where E is the Young's modulus, G is the shear modulus, A is the cross sectional area, J is the polar moment of inertia of the cross section, and ρ is the material's density.

To solve equation (1), a semi-analytical approach is used. In this approach, the time response of the system is written as:

$$u(x,t)=\sum_{i=1}^{p}c_i\eta_i(x)\gamma_i(t) \tag{4}$$

where c_i are real constants,$\eta_i(x)$ are 'appropriate' functions satisfying the essential boundary conditions and $\gamma_i(t)$ are 'appropriate' functions satisfying the initial conditions. For a free-free bar, $\eta_i(x)$ can be:

$$\eta_i(x)=cos\left(\frac{i\pi x}{L}\right),i=1,2,...,p \tag{5}$$

Substituting equation (5) in the equation of motion, multiplying the outcome by η_j and integrating from $x=0$ to $x=L$, yield a set of Ordinary Differential Equations (ODEs) as follows:

$$([M]\ddot{\gamma}+[K]\gamma)\boldsymbol{c}=0 \tag{6}$$

The components of mass and stiffness matrices are given by:

$$M_{ij}=\int_0^L\beta\eta_i\eta_j dx \tag{7}$$

$$K_{ij}=\int_0^L\alpha\eta_i^{'}\eta_j^{'}dx \tag{8}$$

where the prime denotes derivatives with respect to x. Assuming harmonic responses for γ, results in the following eigenvalue problem:

$$\left([K]-[M]\omega^2\right)\boldsymbol{c}=0 \tag{9}$$

Non-trivial solutions of this equation give the natural frequencies (ω). Each natural frequency yields a response vector $\boldsymbol{c}$ based on which the mode shapes can be determined as follows:

$$\Gamma=\sum_{i=1}^{p}c_i\eta_i \tag{10}$$

2.2. Stress analysis

When only a specified mode (e.g. i^{th} mode) of the bar is excited, the longitudinal and torsional deformations will only depend on the corresponding mode shape, i.e.:

$$u(x)=U_0\Gamma_i(x)\gamma_i(t)=U_0\Gamma_i(x)sin(\omega_i t+\theta_0) \tag{11}$$

Assuming the maximum displacement (or rotational angle) at the free ends equals to U_{max} gives the parameter U_0 as:

$$U_0=\frac{U_{max}}{\Gamma_i(0)} \tag{12}$$

Normal stresses for longitudinal vibration and shear stresses for torsional vibration can be obtained by applying Hooke's Law linear elastic response resulting in equations (13) and (14). Strain is derived by the displacement amplitude U_0 and the mode shape vector Γ.

$$\sigma_x=E\frac{\partial u(x)}{\partial x}=EU_0\Gamma_i^{'}(x)\gamma(t) \tag{13}$$

$$\tau_{rx}=Gr\frac{\partial u(x)}{\partial x}=GrU_0\Gamma_i^{'}(x)\gamma(t) \tag{14}$$

in which r in equation (14) is the radial distance from the rod's longitudinal axis. U_0 is the approximate (small rotations) axial displacement induced by the torsional rotation. The highest shear stress is therefore at the outer surface (at the radius) for every cross section.

3. Ultrasonic specimen design and computation

The analytical model described and proposed in this work was used to analyse ultrasonic uniaxial (tension–compression and pure torsion) and multiaxial tension–torsion specimens.

The semi-analytical method proposed here was computed by MATLAB scripts created for this purpose. The scripts allow the analysis of any specimen geometry, whether new or already tested, and facilitate easy and quick dimensional or geometric changes to achieve a final 20 kHz working resonance. It is therefore possible to produce any specimen's concept significantly faster than with Finite Element Analysis (FEA), using an iterative process, since the computational

$$\begin{cases} \sigma(x) = E \bullet A_0 \bullet \zeta(L_1, L_2)\left[\dfrac{\xi\cosh(\xi x) \bullet \cosh(\psi x) - \psi\sinh(\xi x) \bullet \sinh(\psi x)}{cosh^2(\psi x)}\right] for x \le L_2 \\ \sigma(x) = E \bullet k \bullet A_0 \sin(k(L-x)), for L_2 < x \le L \end{cases} \quad (16)$$

method is simpler and less power demanding. This is especially useful and important regarding the design of complex multi-mode specimens, as is the case of the tension–torsion specimens that are addressed in this paper.

The assessment of the proposed analytical method performance starts with a uniaxial axisymmetric hourglass specimen, which analytical method is well-known. Next, a more complex multiaxial tension–torsion specimen is analysed. All geometries in this study were subjected to a modal frequency analysis using the Finite Element Analysis (FEA) Abaqus software with hexahedra quadratic elements. The outputs are resonant frequencies (eigenvalues) and mode shapes (eigenvectors). The mode shapes are expressed in unitary millimetre displacement ratios. Because ultrasonic fatigue experiments typically test linear materials in the elastic regime, the displacement-stress relation, which can be obtained from the computed deformed mode shape, is assumed to be linear.

3.1. Tension-compression specimen

The hourglass specimen's geometry has been used in many previous ultrasonic fatigue testing research. Typical materials range from conventional machined steel [15,21], to aluminium [22] to copper [23,24], and to additive manufactured aluminium, titanium, and other alloys [16,25–27]. The experimental methodology with an axisymmetric hourglass shaped specimen has also been widely validated. The design of the specimen can be done analytically using equations from the published literature or by FEA.

The analytical method also provides the required equations to determine the tension–compression stress amplitudes that are produced from the mode shape deformation, based on displacement measurements conducted experimentally. In the particular case where the stress ratio is $R = -1$, the displacement is typically measured at the free end of the specimen. Fig. 1 presents the specimen's drawing with key general dimensions, a representation of the tension–compression setup (booster-horn-specimen) with the point of displacement measurement indicated (free end). The geometry for a specimen made from AISI P20 steel (density $\rho = 7800 kgm^{-3}$, Young's modulus $E = 202 GPa$ and Poisson's ratio $\nu = 0.30$), which was tested in this study, is also depicted with its physical dimensions.

The Bathias analytical method has been developed considering that the unknown dimension to be determined in Fig. 1 (A) is L_1, while dimensions L_2, R_1 and R_2 are given. These preestablished dimensions L_2, R_1 and R_2 can be set based on existing literature and standards for consistency and validation between different methods [1,2,15,16]. The analytical method determines L1 based on the material properties and a target value for the resonant frequency of the ultrasonic machine (generally $\omega = 20 kHz$). Given that the hourglass specimen has a hyperbolic curvature, the induced displacement and resulting normal stress (for a stress ratio $R = -1$, i.e., no mean stress) can be determined from the following equations:

$$\begin{cases} U(x) = A_0 \bullet \zeta(L_1, L_2)\dfrac{\sinh(\xi x)}{cosh(\psi x)}, for x < L_2 \\ U(x) = A_0 \sin(k(L-x)), for L_2 < x < L \end{cases} \quad (15)$$

where E is the Young's modulus, A_0 is the axial displacement measured at the free end of the specimen as per Fig. 1.B, and k, ζ, ψ and ξ are variables that depend on geometrical dimensions and material properties.

The specimen's final geometry represented in Fig. 1.C was obtained using FEA. Due to the differences between the way FEA and analytical methods derive solutions, the results for the L_1 dimension may be slightly different as well when using different methods. While the FEA model resulted in a 20.4 mm value for L_1 for a 20 kHz approximate frequency, the Bathias analytical method resulted in 20.1 mm for the same dimension. The analytical method being proposed herewith resulted in an L_1 value of 20.65 mm. It must not be forgotten that the method being proposed in this paper is more generalised (as it can be used for pure uniaxial tension–compression, pure torsion and multiaxial tension–torsion), hence it is expected that there are some discrepancies between the different methods.

The distribution of the normalised[1] displacements and stress amplitudes along the length of the specimen and for all three methods are plotted in Fig. 2.

A comparison of the resonant frequencies obtained by different methods was also performed. Table 1 shows all three L_1 dimensions that allow obtaining frequencies closest to 20 kHz for each method[2], being the L_1 20.4 mm the final experimentally tested geometry.

There are no significant differences between the three methods. Both the displacement and stress distributions in Fig. 2 show good agreement between the three methods, where the highest difference is 3 % only. The frequency is also in good agreement with a 1.5 % difference when the Bathias analytical method and the herewith proposed semi-analytical method are compared.

The three methods were further compared to experimental measurements. A strain gauge was attached at the centre of the specimen shown in Fig. 1.C. This is the fatigue testing region (i.e., where the maximum stress occurs). The experimental relationship between the displacement at the free end of the specimen and the stress amplitude at the centre of the specimen was compared with the one determined from the three methods discussed. Results were plotted in Fig. 3 for several different stress amplitudes. The stress amplitude that results from the three non-experimental methods is always higher than the experimental value that is when using a strain gauge. Even though the proposed method has the highest discrepancy, it always stays within an acceptable range of 2.6 %.

3.2. Pure torsion specimen

The first pure torsion ultrasonic testing method utilized two transversely connected horns that enabled an axial displacement to be turned into an angular rotation. This ultrasonic fatigue concept was introduced by Marines et al. [28]. The same setup has since then been employed in other publications such as [9,29,30]. Later, Nikitin et al. [31] employed a torsional piezoelectric actuator that can directly excite the setup with

[1] Data was normalised to ensure a common scale was being used when comparing data and to eliminate any numerical discrepancies between the different methods being used.

[2] The dimensions for L_1 that allow obtaining frequencies closest to 20 kHz for each method are underlined in tables 1 and 2.

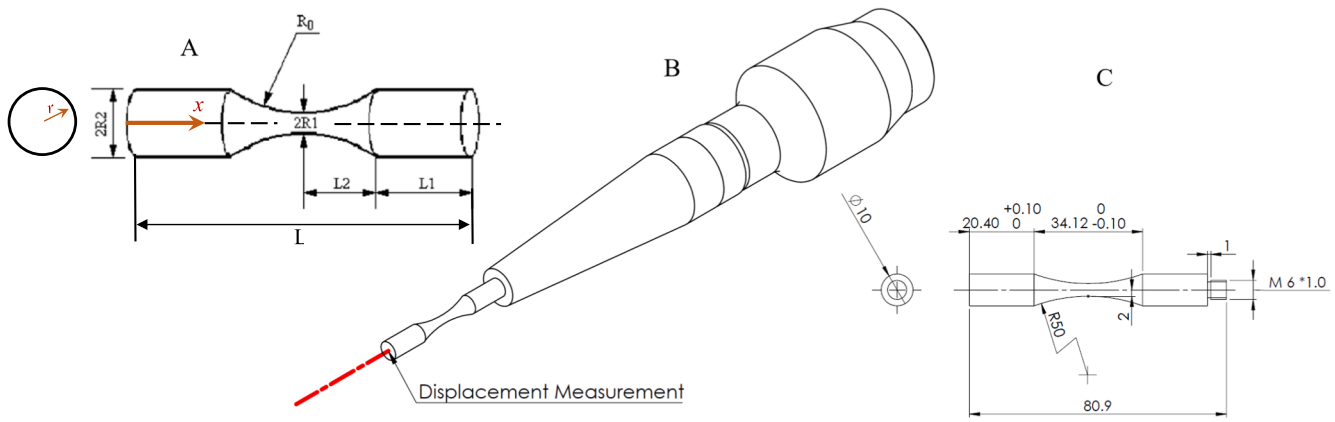

Fig. 1. Tension-compression uniaxial ultrasonic fatigue test specimen and setup: [A] Hourglass specimen key general dimensions; [B] Booster-horn-specimen setup with displacement measurement representation; [C] AISI P20 specimen dimensions. All dimensional units in mm.

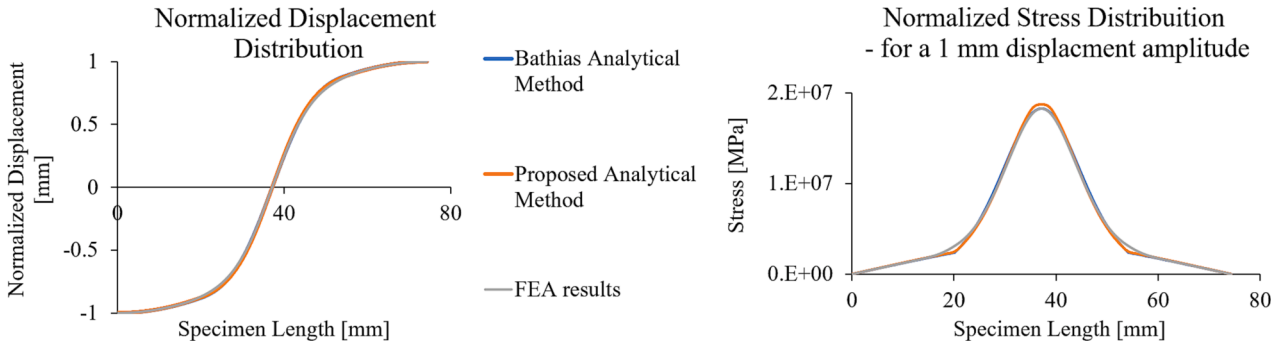

Fig. 2. Tension-Compression specimen 20 kHz mode shape: [A] normalised displacement distribution; [B] resulting normal stress distribution.

Table 1
Tension-compression hourglass specimen modal frequency comparison between the three studied methods.

L1 [mm]	Longitudinal Frequency [kHz]		
	Bathias analytical method	FEA modal analysis	Proposed semi-analytical method
20.1	20.00	20.14	20.25
20.4	19.87	19.98	20.12
20.65	19.76	19.88	20.00

cyclic rotational displacements, discarding the complex two horn design system from Marines.

Both Marines and Nikitin ultrasonic pure torsion methods used the same specimen's geometry. This specimen's shape is very similar to the tension–compression hourglass specimen. The dimensions are determined to achieve not the longitudinal mode, but the rotational/torsional resonant mode at 20 kHz. Therefore, the key rigidity material's property to design the torsional specimen is the shear modulus rather than the Young's modulus. Since the shear modulus has a lower value than the Young's modulus, torsional specimens tend to be smaller than tension–compression specimens.

Again, both Bathias and the Japanese Standard WES 1112:2017 describe an experimental methodology together with analytical equa-

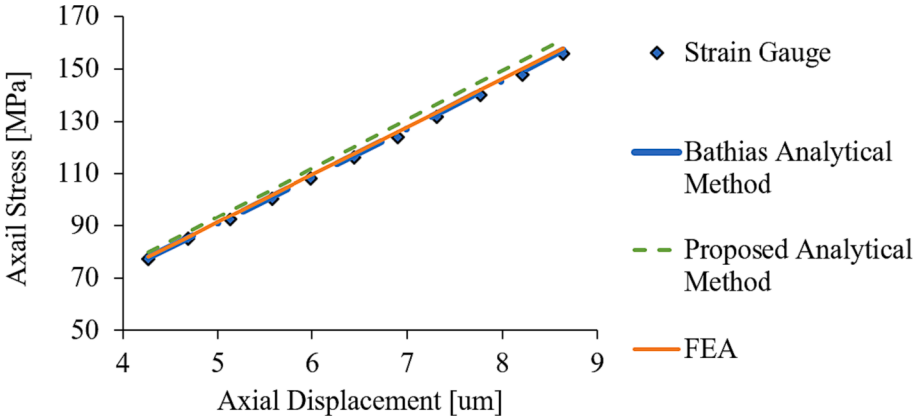

Fig. 3. Tension-compression free-base displacement *vs* stress amplitude at the fatigue region (centre of the specimen for a uniaxial hourglass specimen).

tions for the specimen's design. Equations (17) and (18) are used to calculate the specimen's rotational displacement distribution and the resulting shear stress distribution when the torsional specimen is resonating at a frequency of 20 kHz:

$$\begin{cases} U_r(x) = A_{0r} \bullet R_1 \bullet \varphi(L_1, L_2)\left[\dfrac{\sqrt{\cosh(\alpha x)}\sinh(\beta x)}{\cosh(\alpha x)}\right], for x < L_2 \\ U_r(x) = A_{0r} \bullet R_2 \cos(k(L-x)), for L_2 < x < L \end{cases} \quad (17)$$

$$\begin{cases} \tau(x) = GA_{0r}R_1\varphi(L_1, L_2)\left[\dfrac{\sqrt{\cosh(\alpha x)}\,[\beta\cosh(\beta x)\cosh(\alpha x) - \alpha\sinh(\beta x)\sinh(\alpha x)]}{cosh^2(\alpha x)}\right], for x \le L_2 \\ \tau(x) = GA_{0r}R_2\sin(k(L-x)), for L_2 < x \le L \end{cases} \quad (18)$$

The torsional specimen dimensions for an AISI P20 steel specimen are presented in Fig. 4, together with an uniaxial tension–compression specimen of the same material for comparison. It is clear the size difference due to the considerably lower value of the shear modulus when compared to the Young's modulus (about two fifths for steel).

Again, the three methods being discussed in this paper (Bathias analytical method, FEA method, and the proposed semi-analytical method) were used to compare the resulting displacement and stress distribution for a unitary rotational displacement value at the base of the specimen (see Fig. 5).

The methods present a negligible difference in the results they produce for the pure torsion specimen. When comparing the ratio of shear stress for a unitary rotational displacement at the free end, the proposed method is closest to FEA, with only 0.2 % difference. Bathias analytical method has the highest difference, with a 6 % discrepancy when compared to the proposed method.

3.3. Tension-torsion specimens

Initially, conventional and ultrasonic fatigue testing were mainly focused on uniaxial cyclical loads, such as tension–compression, pure torsion, and pure bending. Multiaxial stresses were later recognised as the leading dynamic stress state in machines and structures [4,32], meaning two directional loads (biaxial stress state) or even three directional loads (triaxial stress state) became a subject of interest in fatigue testing.

To reach multiaxial stresses in ultrasonic machines more complex specimens and setups may be required. Some of the biaxial ultrasonic fatigue methods developed to the present day include the ones from Montalvão and Wren [33], Montalvão et al. [34] and Costa et al. [12] with the application of cruciform specimens that induce from equi-biaxial (in-phase) to pure shear (out-of-phase) tension–compression biaxial stress states (including non-unitary biaxiality ratios); Brugger et al. [14] biaxial bending where a disk-shaped specimen has a 20 kHz bending resonance excited by an axial horn; and Costa et al. [35] tension–torsion axisymmetric specimen that is excited simultaneously in an axial and transverse resonance using a specially designed (patented) horn.

Costa et al. [35] tension–torsion specimen geometry was also used as a case study to analyse the semi-analytical method proposed in this paper. One interesting difference between the design of tension–torsion specimens as the ones from Costa et al. [35] and biaxial UFT cruciform specimens as the ones introduced by Montalvao and Wren [33], is that the former are multi-mode specimens (where two mode shapes need to resonate at the same 20 kHz frequency) whereas the latter are single-mode specimens (i.e., where the biaxial stress at 20 kHz is achieved from a single mode of deformation). Therefore, tension–torsion ultrasonic machines have a setup that uses a complex ultrasonic horn attached to the commonly used longitudinal piezoelectric transducer. The horn-booster setup was specially designed to excite an also unique specimen so that it resonates with both axial and torsional resonant modes simultaneously. Numerical software is essential for the methodical design and experimental method of this study, as there is no

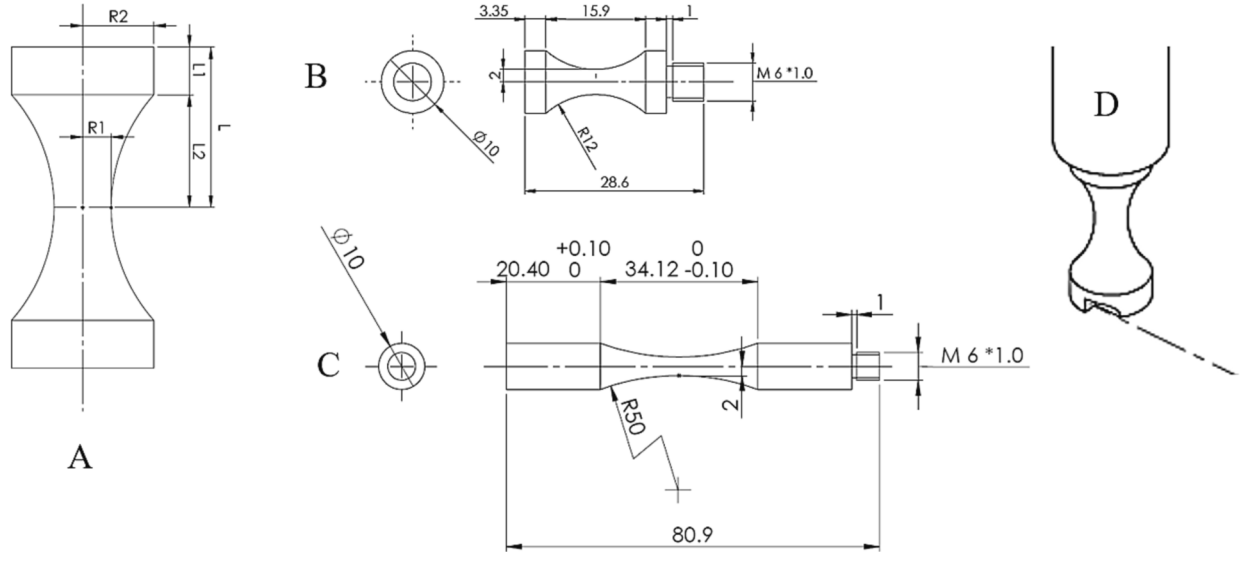

Fig. 4. Pure torsion ultrasonic fatigue test specimen and setup: [A] Hourglass key general dimensions; [B] AISI P20 pure torsion specimen dimensions; [C] AISI P20 tension–compression specimen dimensions; [D] Rotational displacement measurement representation. All dimensional units in mm.

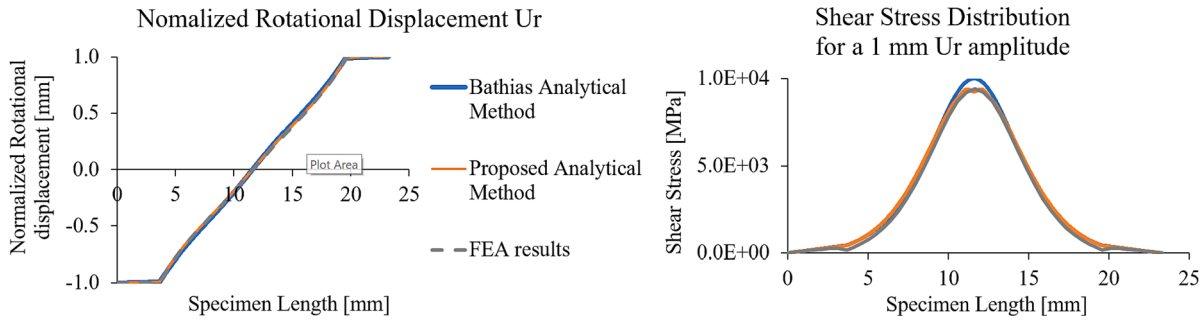

Fig. 5. Pure torsion hourglass 20 kHz mode shape: [A] normalised displacement distribution; [B] resulting normal stress distribution.

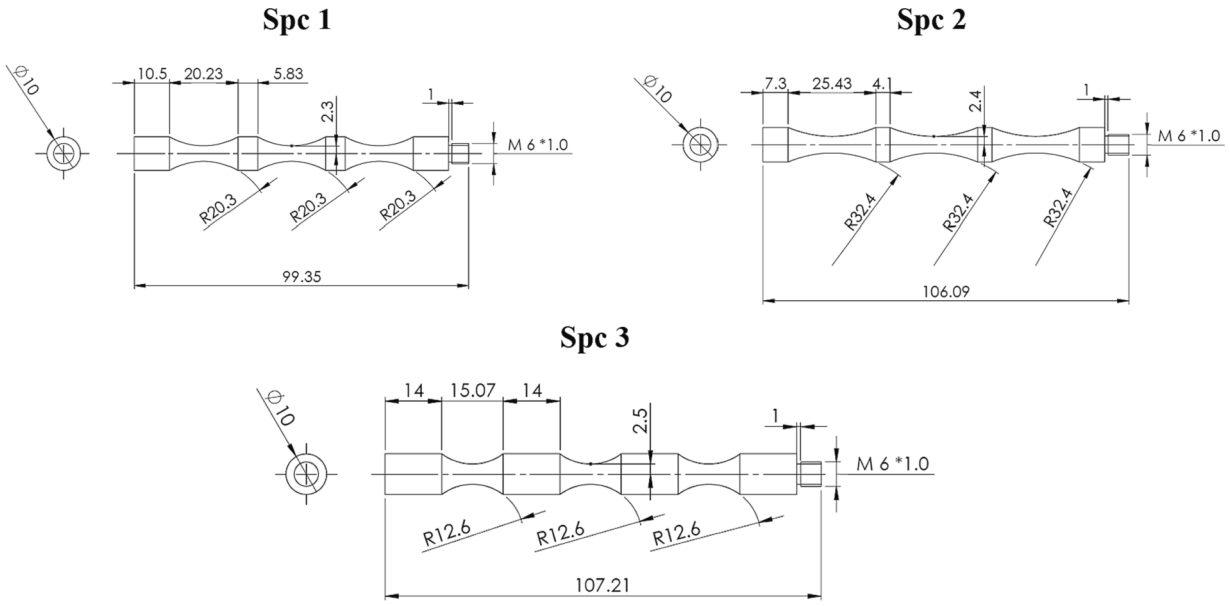

Fig. 6. Costa et al. [36] AISI P20 steel tension–torsion ultrasonic specimen geometries tested. All dimensional units in mm.

Table 2
Pure torsion hourglass specimen modal frequency comparison between the three computed methods.

L1 [mm]	Transverse Frequency [kHz]		
	Bathias analytical method	FEA modal analysis	Proposed semi-analytical method
3.7	20.00	19.29	19.69
3.52	20.34	19.61	20.00
3.35	20.65	19.97	20.37

supporting analytical method, and the resonant behaviour is complex. However, finding a working specimen is very time consuming because of the many variables and the computational time for each specimen iteration. To design a tension–torsion specimen, previous methods required changing the dimensions iteratively until the desired resonant modes and stress ratios were achieved. The resonant modes were 20 kHz for both tension–compression and torsion, and the stress ratio was the intended torsional shear stress divided by the axial normal stress from tension-compression. Fig. 6 presents three AISI P20 steel ultrasonic tension–torsion specimens designed by Costa et al. [36] and which were tested in this study.

All three specimen geometries in Fig. 6 were modelled by iterative FEA computation. By experience knowledge of the effect of each established dimensional variable, each final specimen requires several modal FEA computations before reaching a combination with the two

Table 3
Tension-Torsion ultrasonic specimen modal frequencies comparison between FEA [36] and the proposed analytical method for all three specimen geometries represented in Fig. 6.

	Resonant mode	FEA [kHz]	Proposed Semi-analytical Method [kHz]	Discrepancy (%)
Spc1	Longitudinal	20.00	20.34	1.70
	Torsional	20.02	20.21	0.95
Spc2	Longitudinal	20.00	20.21	1.05
	Torsional	19.99	20.10	0.53
Spc3	Longitudinal	20.04	20.50	2.30
	Torsional	20.05	20.40	1.76

desired resonant modes at 20 kHz, the first longitudinal and the third torsional resonant modes. The frequencies determined for the three specimen designs by FEA (Costa et al. [36]) and the proposed semi-analytical method are compared in Table 3.

From Table 3, the proposed semi-analytical method consistently presents slightly higher frequencies, with a higher frequency difference for the longitudinal resonant mode. Comparing all frequencies, the discrepancies for tension–torsion specimens are slightly larger than for uniaxial specimens (Tables 1 and 2). The results for tension–torsion specimens in Table 3 show a maximum 2.3 % discrepancy between methods, while uniaxial specimens showed maximum discrepancies of 0.7 % and 2 % in Tables 1 and 2 respectively.

Taking as reference specimen Spc2 (the one presenting the best

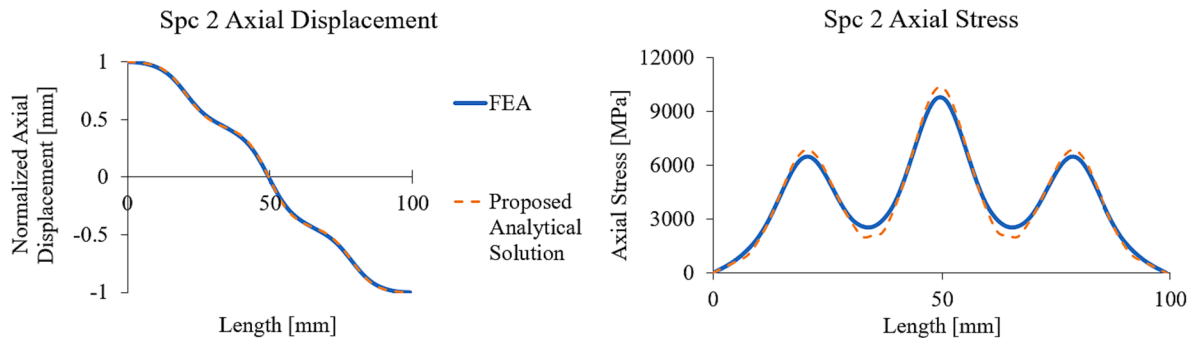

Fig. 7. Spc2 axial displacement and the resulting axial stress distributions.

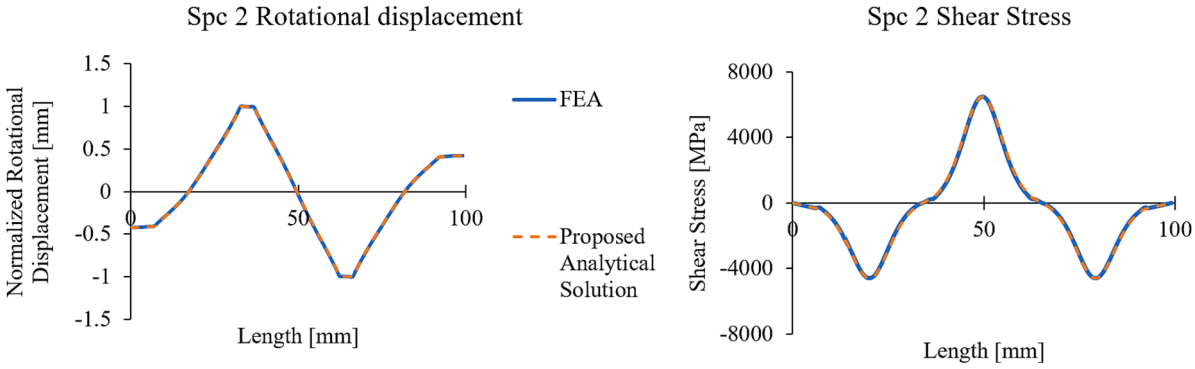

Fig. 8. Spc2 rotational displacement and the resulting shear stress distributions.

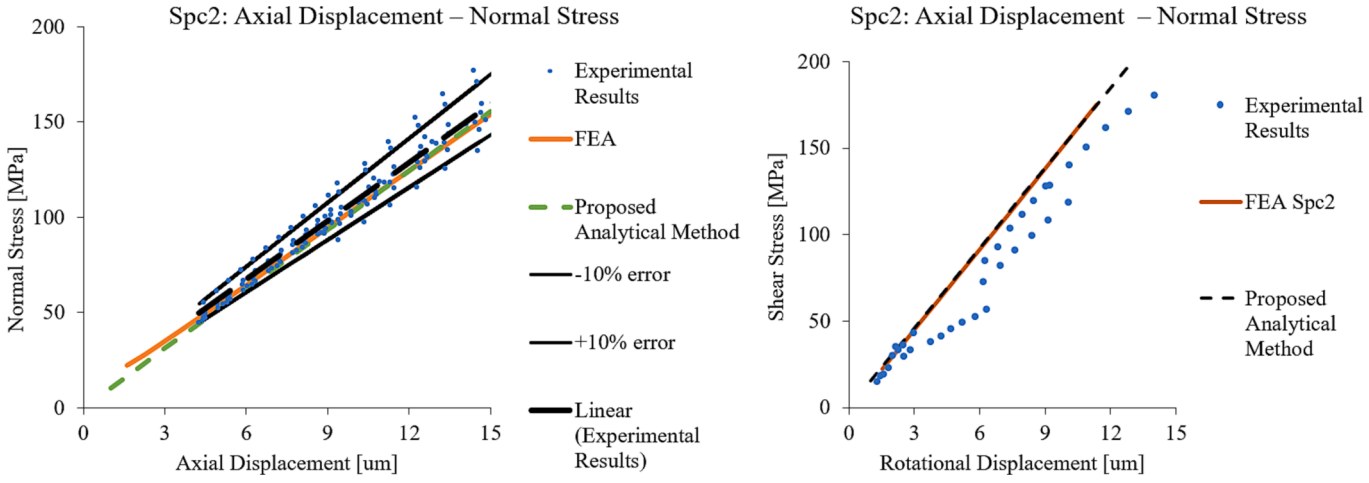

Fig. 9. Tension-Torsion free-base displacement (axial and rotational) *vs* stress amplitude (normal and shear) at the fatigue region (main throat).

agreement between the FEA and the proposed semi-analytical method), Fig. 7 presents the normalized unitary axial displacement and the resulting axial stress distributions, while Fig. 8 presents the normalised unitary rotational displacement and the resulting shear stress distributions.

As with the uniaxial test specimens previously analysed (both tension–compression and pure torsion), the obtained displacement and stress distributions from FEA and the proposed semi-analytical method (Fig. 7) are in good agreement: only a small increase in the induced stress in the fatigue main 'throat' (narrower section) central region is noticed.

Regarding Fig. 8 rotational and resulting shear stress, the same differences as those obtained in the pure torsion specimen are present. The results show even higher agreement both in displacement and resulting stress compared to Fig. 7 axial resonance.

As Costa et al. [36] describe, when testing tension–torsion ultrasonic specimens, both the axial and the rotational displacements at the free end must be measured before conducting the intended fatigue to failure experiments. The resulting measurement methodology consists of the superposition of Fig. 1.B axial measurement and Fig. 4.D rotational measurement. A rosette strain gauge was used by Costa et al. [36] to measure the stress amplitude at the middle of the main 'throat', the highest stress region and therefore the fatigue testing region.

To validate all the methods discussed here for predicting the resonance behaviour of ultrasonic multiaxial specimen geometries, the strains measured by Costa et al. [36] with the placed rosette strain gauges were directly compared for several different imposed amplitudes. A relation between the displacement at the base and the stress at

the 'main throat' was calculated by FEA and the newly proposed semi-analytical method. Using this relation, the stress amplitude can be estimated from the axial and rotational displacements measured in the experiment. Fig. 9 compares all the computed stress state amplitudes in the fatigue testing region of the tension–torsion Spc2 specimen illustrated in Fig. 6 with the experimentally obtained values.

4. Discussion

The semi-analytical method proposed in this paper has demonstrated excellent results. However, this paper does not fully explore the potential of the method. As previously discussed, there is a vast number of ultrasonic fatigue tests that require the redesigning of the specimen geometry towards the intended experiment aims (e.g. size effect [37], fretting [38,39], multiaxial fatigue [4,33–35], etc.). The added complexity beyond the hyperbolic hourglass shape specimens makes the associated analytical calculation cumbersome and unreliable. When under such circumstances, FEA software is used. However, FEA computation is slow, especially when a trial-and-error iterative method is used to reach a final and working geometry. The fast computation of the proposed semi-analytical method makes the design of any future ultrasonic machine components (such as horns and specimens) faster and more reliable. This method can also be interlinked with optimisation methods like the ones presented by Baptista et al. [40,41] for the design of a cruciform geometry.

The tension–torsion specimen was used as a case study to demonstrate the proposed semi-analytical method advantages. When using FEA to obtain the working geometries, a lengthy iterative process is required. However, the presented semi-analytical script can produce the three specimens shown in Fig. 6, along with other combinations, much more quickly, potentially within the same amount of time that an experienced operator would need to produce a single specimen if using FEA.

Beyond the semi-analytical method application presented, there are other applications worth discussing. One example of this semi analytical model optimisation abilities is the modulation of higher critical fatigue volume specimens for size-effect studies. Paolino et al. [37] created several specimens using FEA to reach a 20 kHz ultrasonic specimen that significantly increased the fatigue volume testing region. The application of the proposed method would allow for a fast search of the dimensional combination that presented a given critical fatigue volume, discarding the computational iterative cumbersome FEA process.

Another example is the design of ultrasonic specimens with a constant width narrow section for fretting fatigue, similar to the one applied by Sun et al. [38] or by In-Shik et al. [39]. The analytical equations to determine a final working 20 kHz geometry are a lot more complicated than the ones used for the design of hourglass hyperbolic specimens. When testing specimens for fretting the displacement distribution must be fully characterised to apply the fretting pads in accordance with the desired fretting amplitude.

The semi-analytical method is the same no matter the specimen geometry requirement. Beyond this method only FEA allows for 20 kHz modelling of complex geometries, but this can be more time consuming. The semi-analytical method can also be used as a support for FEA optimisation models for modelling the required specimens. For example, Yoshiaki et al. [42] applied four different specimen geometries (two smooth and two notched) to conduct a fatigue notch effect characterisation of JIS SUJ2-A and SUJ2-B bearing steels. All four specimens were subjected to FEA analysis for determining the final 20 kHz frequency and the stress concentration factor. To achieve the desired stress concentration the FEA software must iteratively produce a 20 kHz working frequency specimen for every variable cross-section until the desired value is meet. The semi-analytical method can be employed to determine several specimen dimensional combinations that yield a 20 kHz resonant frequency, while FEA can be used to determine the resulting stress distribution due to the stress concentration at the notch.

5. Conclusions

The present work introduces a novel semi-analytical method to model both uniaxial and multiaxial ultrasonic fatigue test specimens. The method is based on base functions that satisfy the essential boundary conditions. The computation of the method using MATLAB scripts allows to quickly determine the optimal geometry of the specimens. The performance of the method was tested with uniaxial tension–compression, pure torsion and biaxial tension–torsion ultrasonic specimens. The method provides the frequencies and mode shapes as outputs, including normalised displacement and resulting stress distributions across the specimen's length.

Regarding the uniaxial specimens, the proposed semi-analytical method results were compared with an existing analytical method and Finite Element Analysis (FEA). The results showed the reliability of the method to model a 20 kHz specimen and correctly predict its fatigue stress amplitude for a given measured displacement.

The most interesting application of the method was shown when modelling tension–torsion ultrasonic specimens. Their higher geometric complexity and frequency constraints restrict the application of an analytical method like the one used to determine the geometry of uniaxial specimens. Tension-torsion specimens are multi-mode specimens, i.e., where the specimens are designed so that two mode shapes of interest resonate at the same 20 kHz frequency. Until now, this enforced the application of FEA software, which resulted in a difficult and time-consuming modelling methodology due to the iterative nature of the tuning process. The semi-analytical method proposed in this paper can compute faster than other existing methods. This enables to solve more complex problems involving ultrasonic modulation of specimens. Moreover, it makes it easier to apply this method in optimisation processes.

CRediT authorship contribution statement

Pedro R. da Costa: Conceptualization, Methodology, Validation, Formal analysis, Investigation, Data curation, Visualization, Writing - original draft. **Masoud Rahaeifard:** Conceptualization, Methodology, Software, Formal analysis, Validation, Data curation, Investigation, Writing - review & editing. **Diogo Montalvão:** Conceptualization, Supervision, Project administration, Funding acquisition, Investigation, Writing - review & editing. **Luís Reis:** Conceptualization, Supervision, Project administration, Funding acquisition, Investigation, Writing - review & editing. **Manuel Freitas:** Conceptualization, Supervision, Funding acquisition, Investigation.

Declaration of Competing Interest

The authors declare the following financial interests/personal relationships which may be considered as potential competing interests: Luis Reis reports financial support was provided by Portuguese Foundation for Science and Technology. Diogo Montalvao reports financial support was provided by Research England.

Data availability

Data will be made available on request.

Acknowledgements

This work was supported by FCT (Fundação para a Ciência e a Tecnologia, Portugal), through IDMEC, under LAETA, project UIDB/50022/2020, and by Research England (United Kingdom), through the ADDISONIC's Bournemouth University Strategic Investment Area.

References

[1] Furuya Y, Shimamura Y, Takanashi M, Ogawa T. Standardization of an ultrasonic fatigue testing method in Japan. Fatigue Frac. Eng Mater Struct 2022;45:2415–20. https://doi.org/10.1111/ffe.13727.

[2] Japan Welding Engineering Society. Standard method for ultrasonic fatigue test in metallic materials. WES 1112; 2017.

[3] Mason WP, Baerwald H. Piezoelectric crystals and their applications to ultrasonics. Phys Today 1951;4:23–4. https://doi.org/10.1063/1.3067231.

[4] Costa P, Nwawe R, Soares H, Reis L, Freitas M, Chen Y, et al. Review of multiaxial testing for very high cycle fatigue: from "Conventional" to ultrasonic machines. Machines 2020:8. https://doi.org/10.3390/MACHINES8020025.

[5] Furuya Y, Takeuchi E. Gigacycle fatigue properties of Ti-6Al-4V alloy under tensile mean stress. Mater Sci Eng A 2014;598:135–40. https://doi.org/10.1016/j.msea.2014.01.019.

[6] Kovacs S, Beck T, Singheiser L. Influence of mean stresses on fatigue life and damage of a turbine blade steel in the VHCF-regime. Int J Fatigue 2013. https://doi.org/10.1016/j.ijfatigue.2012.12.012.

[7] Koster M, Wagner G, Eifler D. Cyclic deformation behaviour of a medium carbon steel in the VHCF regime. Proc Eng 2010. https://doi.org/10.1016/j.proeng.2010.03.235.

[8] Xue HQ, Bathias C. Crack path in torsion loading in very high cycle fatigue regime. Eng Fract Mech 2010;77:1866–73. https://doi.org/10.1016/j.engfracmech.2010.05.006.

[9] Schuller R, Mayer H, Fayard A, Hahn M, Bacher-Höchst M. Very high cycle fatigue of VDSiCr spring steel under torsional and axial loading. Materwiss Werksttech 2013;44:282–9. https://doi.org/10.1002/mawe.201300029.

[10] Xue HQ, Tao H, Montembault F, Wang QY, Bathias C. Development of a three-point bending fatigue testing methodology at 20 kHz frequency. Int J Fatigue 2007;29:2085–93. https://doi.org/10.1016/j.ijfatigue.2007.03.018.

[11] Adam TJ, Horst P. Experimental investigation of the very high cycle fatigue of GFRP [90/0]s cross-ply specimens subjected to high-frequency four-point bending. Compos Sci Technol 2014;101:62–70. https://doi.org/10.1016/j.compscitech.2014.06.023.

[12] da Costa PR, Reis L, Montalvão D, Freitas M. A new method for ultrasonic fatigue testing of equibiaxial and pure shear cruciform specimens. Int J Fatigue 2021:152. https://doi.org/10.1016/j.ijfatigue.2021.106423.

[13] Costa PR, Montalvão D, Freitas M, Baxter R, Reis L. Cruciform specimens' experimental analysis in ultrasonic fatigue testing. Fatigue Fract Eng Mater Struct 2019;42:2496–508. https://doi.org/10.1111/ffe.13041.

[14] Brugger C, Palin-Luc T, Osmond P, Blanc M. Gigacycle fatigue behaviour of a cast aluminum alloy under biaxial bending: experiments with a new piezoelectric fatigue testing device. Proc Struct Integr 2016;2:1179–80. https://doi.org/10.1016/j.prostr.2016.06.150.

[15] Marines I, Dominguez G, Baudry G, Vittori JF, Rathery S, Doucet JP, et al. Ultrasonic fatigue tests on bearing steel AISI-SAE 52100 at frequency of 20 and 30 kHz. Int J Fatigue 2003;25:1037–46. https://doi.org/10.1016/S0142-1123(03)00161-0.

[16] da Costa PR, Sardinha M, Reis L, Freitas M, Fonte M. Ultrasonic fatigue testing in as-built and polished Ti6Al4V alloy manufactured by SLM. Forces Mech 2021;4:100024. https://doi.org/10.1016/j.finmec.2021.100024.

[17] Ding J, Cheng L. Experimental study on ultrasonic three-point bending fatigue of CFRP under ultraviolet radiation. Eng Fract Mech 2021:242. https://doi.org/10.1016/j.engfracmech.2020.107435.

[18] Reß W, Khatibi G, Weiss B, Gröger V. An ultrafast mechanical test system for bending fatigue studies of multilayered electronic components. In: 2012 4th electronic system-integration technology conference, ESTC 2012; 2012. doi: 10.1109/ESTC.2012.6542197.

[19] Bathias C, Paris PC. Gigacycle fatigue in mechanical practice; 2005. doi: 10.1201/9780203020609.

[20] Mohammadi Arani E, Rahaeifard M. A nonclassical formulation for torsion of variable cross section functionally graded microbars. Acta Mech 2022;233:3481–95. https://doi.org/10.1007/s00707-022-03288-2.

[21] Tridello A, Paolino DS, Chiandussi G, Rossetto M. Effect of electroslag remelting on the VHCF response of an AISI H13 steel. Fatigue Fract Eng Mater Struct 2017;40:1783–94. https://doi.org/10.1111/ffe.12696.

[22] Mayer H, Fitzka M, Schuller R. Constant and variable amplitude ultrasonic fatigue of 2024–T351 aluminium alloy at different load ratios. Ultrasonics 2013. https://doi.org/10.1016/j.ultras.2013.02.012.

[23] Stanzl-Tschegg S, Mughrabi H, Schoenbauer B. Life time and cyclic slip of copper in the VHCF regime. Int J Fatigue 2007;29:2050–9. https://doi.org/10.1016/j.ijfatigue.2007.03.010.

[24] Stanzl-Tschegg SE. Influence of material properties and testing frequency on VHCF and HCF lives of polycrystalline copper. Int J Fatigue 2017;105:86–96. https://doi.org/10.1016/j.ijfatigue.2017.08.014.

[25] Tridello A, Fiocchi J, Biffi CA, Chiandussi G, Rossetto M, Tuissi A, et al. VHCF response of heat-treated SLM Ti6Al4V Gaussian specimens with large loaded volume. Proc Struct Integr 2019;18:314–21. https://doi.org/10.1016/j.prostr.2019.08.171.

[26] Günther J, Krewerth D, Lippmann T, Leuders S, Tröster T, Weidner A, et al. Fatigue life of additively manufactured Ti–6Al–4V in the very high cycle fatigue regime. Int J Fatigue 2017;94:236–45. https://doi.org/10.1016/j.ijfatigue.2016.05.018.

[27] Siddique S, Imran M, Wycisk E, Emmelmann C, Walther F. Fatigue assessment of laser additive manufactured AlSi12 eutectic alloy in the very high cycle fatigue (VHCF) range up to 1E9 cycles. Mater Today: Proc 2016;3:2853–60. https://doi.org/10.1016/j.matpr.2016.07.004.

[28] Marines-Garcia I, Doucet JP, Bathias C. Development of a new device to perform torsional ultrasonic fatigue testing. Int J Fatigue 2007;29:2094–101. https://doi.org/10.1016/j.ijfatigue.2007.03.016.

[29] Bayraktar E, Xue H. Torsional fatigue behaviour and damage mechanisms in the very high cycle regime. Arch Mater Sci Eng 2010;43:77–86.

[30] Xue HQ, Bayraktar E, Marines-garcia I, Bathias C. Torsional fatigue behaviour in gigacycle regime and damage mechanism of the perlitic steel. J Achiev Mater Manuf Eng 2008;31:391–7.

[31] Nikitin A, Bathias C, Palin-Luc T. A new piezoelectric fatigue testing machine in pure torsion for ultrasonic gigacycle fatigue tests: Application to forged and extruded titanium alloys. Fatigue Fract Eng Mater Struct 2015;38:1294–304. https://doi.org/10.1111/ffe.12340.

[32] de Freitas M. Multiaxial fatigue: from materials testing to life prediction. Theor Appl Fract Mech 2017;92:360–72. https://doi.org/10.1016/j.tafmec.2017.05.008.

[33] Montalvão D, Wren A. Redesigning axial-axial (biaxial) cruciform specimens for very high cycle fatigue ultrasonic testing machines. Heliyon 2017;3:e00466.

[34] Montalvão D, Blaskovics A, da Costa R, Reis L, Freitas M. Numerical analysis of VHCF cruciform test specimens with non-unitary biaxiality ratios. Int J Comput Methods Exp Measur 2019;7:327–39. https://doi.org/10.2495/CMEM-V7-N4-327-339.

[35] Costa P, Vieira M, Reis L, Ribeiro A, de Freitas M. New specimen and horn design for combined tension and torsion ultrasonic fatigue testing in the very high cycle fatigue regime. Int J Fatigue 2017;103:248–57. https://doi.org/10.1016/j.ijfatigue.2017.05.022.

[36] da Costa PR, Reis L, Freitas M. Very high cycle fatigue under tension/torsion loading of mold low alloy steel. Fatigue Fract Eng Mater Struct 2022. https://doi.org/10.1111/ffe.13907.

[37] Paolino DS, Tridello A, Chiandussi G, Rossetto M. On specimen design for size effect evaluation in ultrasonic gigacycle fatigue testing. Fatigue Fract Eng Mater Struct 2014;37:570–9. https://doi.org/10.1111/ffe.12149.

[38] Sun ZD, Bathias C, Baudry G. Fretting fatigue of 42CrMo4 steel at ultrasonic frequency. Int J Fatigue 2001;23:449–53. https://doi.org/10.1016/S0142-1123(00)00097-9.

[39] Cho IS, Lee CS, Amanov A, Pyoun YS, Park IG. The effect of ultrasonic nanocrystalline surface modification on the high-frequency fretting wear behaviour of AISI304 steel. J Nanosci Nanotechnol 2011;11:742–6. https://doi.org/10.1166/jnn.2011.3219.

[40] Baptista R, Reis L, Guelho I, Freitas M, Madeira JFA. Design optimization of cruciform specimens for biaxial fatigue loading. Frattura Ed Integrita Structurale 2014;30:118–26. https://doi.org/10.3221/IGF-ESIS.30.16.

[41] Baptista R, Claudio RA, Reis L, Madeira JFA, Guelho I, Freitas M. Optimization of cruciform specimens for biaxial fatigue loading with direct multi search. Theor Appl Fract Mech 2015;80:65–72. https://doi.org/10.1016/j.tafmec.2015.06.009.

[42] Akiniwa Y, Miyamoto N, Tsuru H, Tanaka K. Notch effect on fatigue strength reduction of bearing steel in the very high cycle regime. Int J Fatigue 2006;28:1555–65. https://doi.org/10.1016/j.ijfatigue.2005.04.017.